ChemPhysChem

Research Article
doi.org/10.1002/cphc.202200443

Chemistry Europe
European Chemical Societies Publishing

www.chemphyschem.org

Theoretical and Experimental Determination of Thermomechanical Properties of Epoxy-SiO_2 Nanocomposites

Mohammed Mostafa Adnan[+],[a] Arpenik Kroyan[+],[a] Chaman Srivastava,[b] Sotirios Grammatikos,[b] Julia Glaum,[a] Marit-Helen Glomm Ese,[c] Sondre Kvalvåg Schnell,[a] and Mari-Ann Einarsrud*[a]

Improvements in the thermomechanical properties of epoxy upon inclusion of well-dispersed SiO_2 nanoparticles have been demonstrated both experimentally and through molecular dynamics simulations. The SiO_2 was represented by two different dispersion models: dispersed individual molecules and as spherical nanoparticles. The calculated thermodynamic and thermomechanical properties were consistent with experimental results. Radial distribution functions highlight the interactions of different parts of the polymer chains with the SiO_2 between 3 and 5 nm into the epoxy, depending on the particle size. The findings from both models were verified against experimental results, such as the glass transition temperature and tensile elastic mechanical properties, and proved suitable for predicting thermomechanical and physicochemical properties of epoxy-SiO_2 nanocomposites.

Introduction

Epoxy-based nanocomposites are promising materials for use in power transmission equipment as high voltage insulation due to the potential improvements in their dielectric, thermal, and mechanical properties compared to pure epoxy.[1] Several types of inorganic nanoparticles (*e.g.*, SiO_2, TiO_2, BN, SiC, MgO, ZnO, and Al_2O_3) have been employed as filler materials in epoxy, with varying degrees of success.[1] The type of material is not as crucial for the dielectric properties[2] as the state of dispersion of the nanoparticles.[3] Molecular dynamics (MD) simulations have been widely used to predict the properties of polymeric materials with and without inorganic fillers.[4–7] The effects of nanoparticle size, composition, and morphology on the thermal and mechanical properties of the nanocomposites can be investigated using MD simulations, which can complement experimental measurements of, *e.g.*, dielectric properties. Simulations can be a powerful tool in selecting the inorganic component in epoxy nanocomposites which can be used to improve the thermomechanical properties. Nevertheless, the accuracy of predictions is highly dependent on the choice of model.[8,9] While most simulations on epoxy systems use the same monomer for the epoxy resin (diglycidyl ether of bisphenol-A (DGEBA)), variations are found in the type of cross-linking agents and force fields used in the simulations.[10–17] The approach used in the cross-linking procedure can also affect the structure's equilibration and the computational time.[12] Over the last decade, several models have been created for epoxy-SiO_2 interfaces to simulate thermomechanical properties, *e.g.*, flat layers,[18,19] nanoparticles of various sizes,[14] shapes,[20,21] and surface grafting.[14,15,22] Despite these efforts, overestimation of elastic modulus, glass transition temperature and thermal conductivity present challenges to MD simulations of hybrid epoxy-SiO_2 materials.

This work investigates the thermal and thermomechanical properties of pure epoxy and epoxy-SiO_2 nanocomposites cross-linked with an amine-based curing agent using MD simulations. The simulations were performed using the OPLS/CM1A force field for the epoxy, which includes accurate charge models for reproducing experimental properties.[23,24] Figures 1a and 1b show the structures of the models used for the epoxy resin (DGEBA) and the curing agent (poly(oxypropylene) diamine), respectively. Figures 1c and 1d illustrate the two representations of the SiO_2. Model I represents the SiO_2 as amorphous, sphere-like nanoparticles with varying sizes and 3 or 4-coordinated Si atoms (tertiary and quaternary Si, respectively) with covalent bonds forming the Si–O–Si network. Model II represents the SiO_2 as individual molecules that form non-spherical amorphous clusters (instead of grouping together to form a single nanoparticle of defined size), with varying filler content. In both models, the basic building block of the SiO_2 are bent O–Si–O units that form amorphous structures. However, the distribution of SiO_2 in Model I is uniform, whereas

[a] Dr. M. M. Adnan,[+] A. Kroyan,[+] Dr. J. Glaum, Dr. S. K. Schnell, Dr. M.-A. Einarsrud
Department of Materials Science and Engineering
NTNU Norwegian University of Science and Technology
7491 Trondheim, Norway
E-mail: mari-ann.einarsrud@ntnu.no
[b] C. Srivastava, Dr. S. Grammatikos
Laboratory for Advanced and Sustainable Engineering Materials (ASEMlab), Department of Manufacturing and Civil Engineering
NTNU Norwegian University of Science and Technology
2815 Gjøvik, Norway
[c] Dr. M.-H. Glomm Ese
SINTEF Energy Research AS
7034 Trondheim, Norway
[+] These authors contributed equally to this work

Supporting information for this article is available on the WWW under https://doi.org/10.1002/cphc.202200443

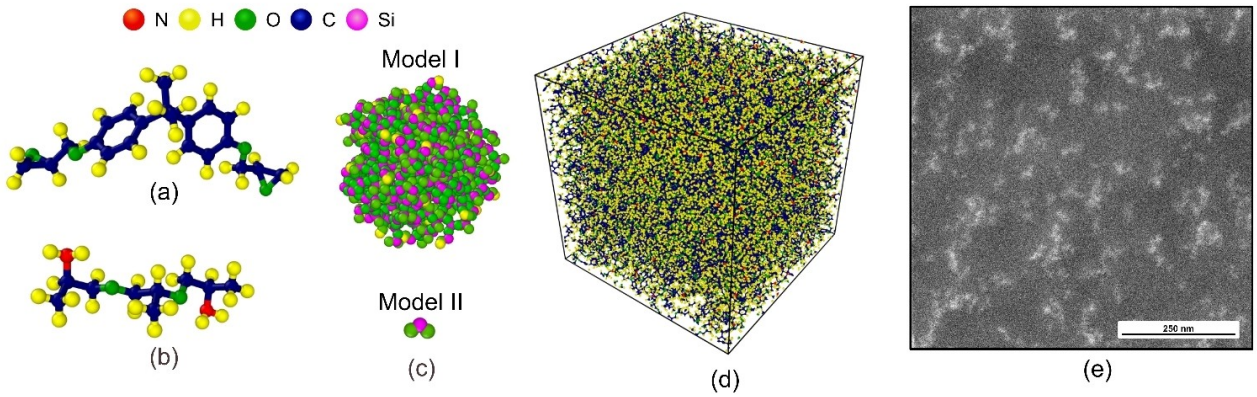

Figure 1. Representations of the molecular models for (a) DGEBA monomers, (b) poly(oxypropylene) diamine monomers, and (c) the SiO_2 nanoparticle used in Model I (top) and the SiO_2 unit used in Model II. (d) The cross-linked unit cell used for simulations of pure epoxy. (e) High angle annular dark-field STEM image of epoxy nanocomposite *in situ* synthesized with 5 wt% SiO_2, showing the state of dispersion of the nanoparticles (shown as bright areas or spots).

in Model II it is random. Figure 1d depicts a representative unit cell of the nanocomposite after the cross-linking of epoxy.

The calculated thermal and tensile properties were benchmarked using experimental results from nanocomposites prepared by *in situ* synthesized SiO_2.[25] The microstructure of the synthesized nanocomposite with 5 wt% SiO_2 is shown in Figure 1e, exhibiting well-dispersed SiO_2 clusters between 50 and 100 nm.

The O–Si–O molecule is chosen for these models instead of quartz as the nanocomposites containing SiO_2 prepared via *in situ* methods will contain amorphous SiO_2 and not crystalline quartz. The clusters formed by the O–Si–O units in Model II also form irregular structures in the polymer matrix resembling that observed in the real nanocomposites.[25,26]

Results and Discussion

Organic-inorganic Interface

Radial distribution functions (RDFs) calculated for the Si atoms in both models show the density and distribution of different atoms around the Si atoms. Selected RDFs for Model I and II are displayed in Figure 2. Figures 2a and 2b show the RDFs for quaternary Si atoms (in Model I) with reacted amine groups in the cross-linked epoxy (labelled as NCC in the figures) as well as the oxygen atoms in DGEBA molecules (labelled as O-polymer).

Figures 2b and 2c show the corresponding RDFs for tertiary Si atoms. The RDFs for the Si atoms in Model II with both the oxygen in neighbouring SiO_2 units and the oxygen in DGEBA are shown in Figures 2e and 2f, respectively.

The structure of the tertiary and quaternary Si atoms shown in Figure 3 results from the procedure used to build the nanoparticles using Model I and is described in further detail in the Supplementary Information. Typically, the nanoparticles consist of 60–80% tertiary Si and 20–40% quaternary Si. The coordination number of tertiary amines and the oxygen in the DGEBA to tertiary and quaternary Si atoms in Model I decreased with increasing size of the SiO_2 nanoparticle. This is indicated by the change from sharp individual peaks to broad and diffuse signals in the RDFs.

The decrease in the coordination number of atoms from different parts of the polymer to the Si atoms with increasing particle size emphasizes the importance of particle size on the interface properties. This decrease shows that comparatively fewer polymer chains are within proximity of each individual Si atom on the surface as the particles get larger. Therefore, there are fewer interactions per unit area between the SiO_2 and the polymer chains, which affects the properties. This behaviour is also replicated for the RDFs of the Si to the other parts of the polymer (*e.g.*, unreacted epoxide groups or amine groups in DGEBA or the curing agent, respectively), which are shown in the Supplementary Information.

The SiO_2 units in Model II show consistent RDFs with changes in the filler content (wt%). No significant differences are observed concerning the organization of the polymer chains around the SiO_2, as seen in Figure 2f. However, some degree of clustering was observed from the RDFs of the oxygen from SiO_2 units. The strong signal at 1.8 Å corresponds to the oxygen atoms directly bonded to Si in each SiO_2 unit and is the same in all cases, but the broad peak at 4–6 Å varies with filler content. The number of neighbouring SiO_2 units surrounding each SiO_2 molecule decreases between 1 and 3 wt%, and then increases again between 3 and 5 wt%. A similar trend is observed and replicated in the RDFs between Si atoms in the SiO_2, indicating that the SiO_2 units in Model II appear to be closer to one another at both 1 and 5 wt%. However, at 3 wt% they are further apart and more dispersed.

The coordination numbers of different atoms around the Si atoms obtained from the RDFs (Table 1) show that the ends of the polymer molecules (both DGEBA and the curing agent) appear to be more frequent around the SiO_2 than the central parts of the polymers. For example, there are more amines from the curing agent and terminal carbon atoms from the epoxide rings of DGEBA around the SiO_2 than atoms from the aromatic rings of the DGEBA. The RDFs can also be used to estimate how

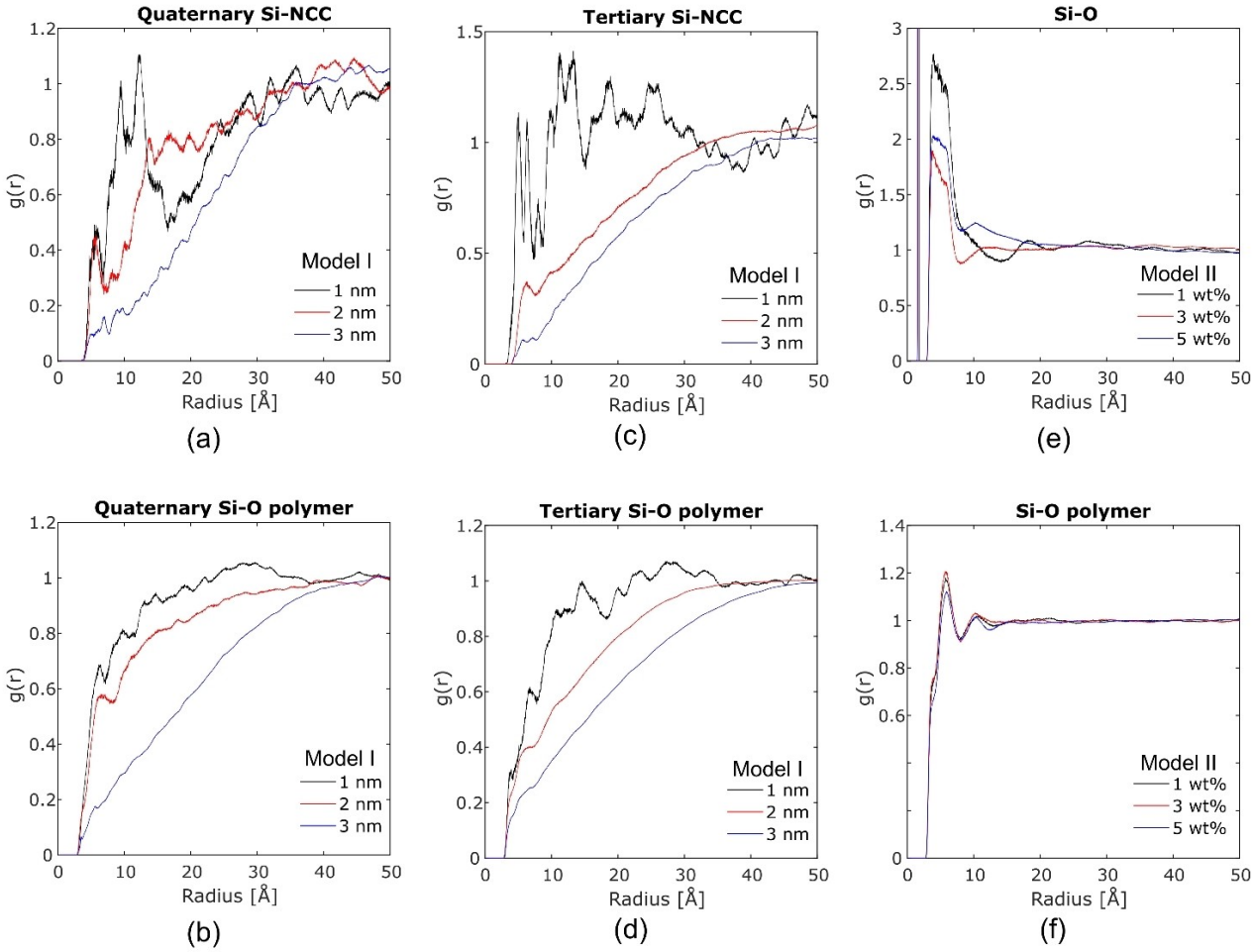

Figure 2. Radial distribution functions for quaternary Si atoms in Model I with (a) reacted amines (NCC) and (b) oxygen atoms in DGEBA chains, for (c) Si atoms in Model II with oxygen from other SiO_2 molecules, for tertiary Si atoms in Model I with (d) reacted amines (NCC) and (e) oxygen atoms in DGEBA chains, and for (f) Si atoms in Model II with oxygen atoms in DGEBA chains. The sizes of the nanoparticles in Model I are shown in the legend.

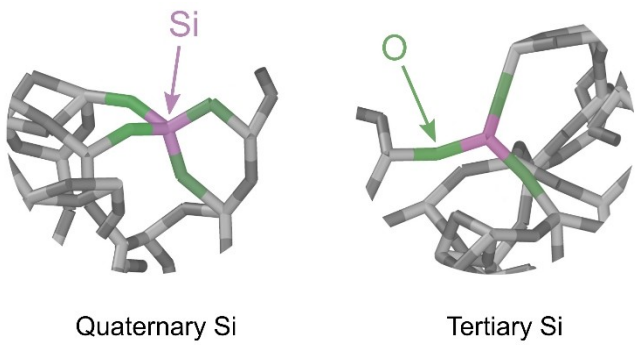

Figure 3. Illustration showing quaternary and tertiary Si atoms bonded to 4 and 3 oxygens, respectively, in the SiO_2 nanoparticles constructed in Model I.

Table 1. Coordination numbers of selected atoms with respect to Si atoms at a distance corresponding to the first peak in the respective RDFs from Model I and II.

System	N[a]	H[b]	C[c]	O[d]	NCC[e]	Si[f]	O[g]
Model I quaternary Si atoms							
1 nm	3.2	0.6	1.6	1.9	1	–	–
2 nm	1.6	0.9	1.2	2.4	0.8	–	–
3 nm	1.4	0.1	0.6	0.3	0.4	–	–
Model I tertiary Si atoms							
1 nm	1	0.1	2.9	2.1	2.1	–	–
2 nm	2.1	0.5	1.5	1.4	1.4	–	–
3 nm	1.4	0.2	0.7	0.8	0.8	–	–
Model II							
1 wt%	6.5	4	4	4.6	4.7	9.6	9.6
3 wt%	5.3	4.3	4.3	4.7	4.9	6.5	6.4
5 wt%	5.1	3.9	3.9	4.3	4.4	7.7	7.5

[a] Primary amine (N) in unreacted curing agent. [b] H in aromatic rings in DGEBA. [c] Terminal C in unreacted epoxide group in DGEBA. [d] O in C–O-C ether group in DGEBA. [e] Tertiary amine (N) in POPDA linked to two DGEBA molecules. [f] Si atoms in SiO_2 molecular units. [g] O in SiO_2 molecular units.

far the interfacial region between the polymer chains and the SiO_2 nanoparticles extends. Figure 2 shows that *g(r)* approaches 1 in the range 30–50 Å in Model I, depending on the particle size – therefore, the polymer chains up to this distance are most affected by the SiO_2 surface, while those beyond are

Table 2. Comparison of thermal and mechanical properties of epoxy and its nanocomposites determined both experimentally and calculated from MD simulations.

SiO_2 content [wt%]	T_g (DSC) [°C]	T_g (DMA) [°C]	T_g (MD) [°C] Model I	Model II	Elastic modulus (experimental) [GPa]	Elastic modulus (MD) [GPa] Model I	Model II	Thermal conductivity (MD) [$W m^{-1} K^{-1}$] Model I	Model II
0	83	81		97[a] 66[b]	2.49 ± 0.20	3.78 ± 0.08[a] 2.29 ± 0.03[b]		0.44[a] 0.38[b]	
1	72	61	55	84	2.01 ± 0.43	2.35 ± 0.05	3.37 ± 0.07	0.32	1.16
3	75	56	–	73	2.38 ± 0.61	–	2.14 ± 0.02	–	1.22
5	87	66	64	96	3.06 ± 0.61	2.54 ± 0.05	3.33 ± 0.08	0.45	1.77
15	–	–	89	–	–	2.75 ± 0.6	–	0.62	–

[a] 90% cross-linked. [b] 60% cross-linked.

arranged more homogeneously and are unaffected by the particle (resulting in the uniform density distribution in the RDF). However, neither of the models include covalently bonded interactions between the SiO_2 and the epoxy chains, which are known to influence the interface significantly.[27] Such interactions may be included in the simulations via the incorporation of coupling agents, such as those used in the nanocomposites prepared experimentally, or other surface modifiers in future developments of Model I.

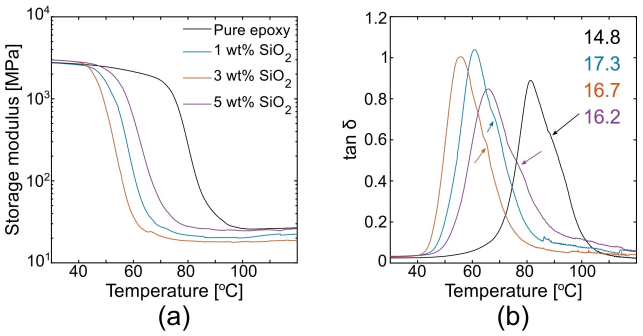

Figure 4. (a) Storage modulus, and (b) loss tangent (tan δ) of pure epoxy and epoxy-SiO_2 nanocomposites. The arrows in (b) show the positions of the shoulders on the tan δ peaks, and the numbers correspond to the areas underneath the peaks.

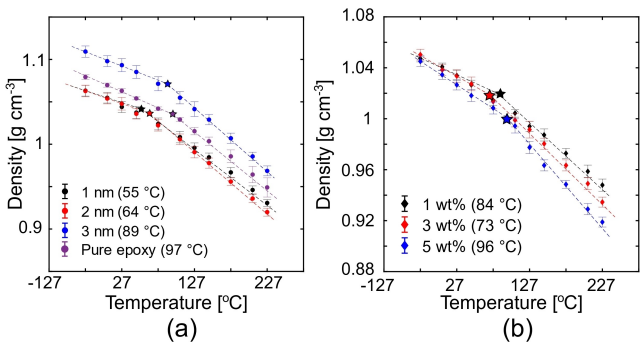

Figure 5. Simulated changes in density with temperature for (a) pure epoxy and epoxy-SiO_2 nanocomposites using model I, and (b) model II. The asterisks show the estimation of T_g, which is reported in the legend.

Thermal and Mechanical Properties

Table 2 summarises the measured thermal and mechanical properties, compared to the simulated equivalents, of pure epoxy and nanocomposites with varying SiO_2 contents. The glass transition temperature (T_g) was experimentally observed to initially decrease with the addition of SiO_2, before subsequently increasing at higher filler contents. Data from differential scanning calorimetry (DSC) and dynamic mechanical analysis (DMA) exhibit the same trend, although the values for each temperature differed between the two methods. The observed trend in T_g was attributed to the formation of mass fractal SiO_2 morphologies for a low amount of SiO_2,[25] resulting in a plasticizing effect on the surrounding epoxy. The storage modulus and tan δ from DMA for nanocomposites with different amounts of SiO_2 are shown in Figure 4. A shoulder is observed on the tan δ peak at the high-temperature side in both the pure epoxy and nanocomposites. These tan δ features indicate differences in cross-linking density in the heterogeneous regions in the cured resins. The height of the tan δ peaks is also observed to exhibit a similar trend to the T_g, where the peak is initially larger at low SiO_2 content and then decreasing below that of pure epoxy at higher content (5 wt%). Therefore, with sufficient SiO_2 the nanocomposites exhibit a stiffer response. Additionally, the area underneath the tan δ peak (shown in Figure 4b) is larger in the nanocomposites than in pure epoxy, which corresponds to an improved damping ability of the nanocomposites, allowing them to absorb and dissipate energy more effectively. The expected disparity between the T_g values obtained from DSC and DMA are attributed to the nature of the two methods.

The changes in density with temperature in the simulated epoxy and epoxy-SiO_2 nanocomposite systems are shown in Figure 5. The glass transition can be identified from the region where the slope of the linear plots changes. The T_g obtained from the MD simulations also exhibits the same trends observed experimentally. This behaviour was replicated in both the models, but the values for T_g obtained varied significantly between them. In Model I, consisting of SiO_2 in particulate form, T_g values were closer to those obtained from DMA, as seen in Table 2. Meanwhile, the T_g values obtained from Model II, with molecular SiO_2, are closer to those obtained from the DSC data. The differences in the obtained values for T_g can be attributed

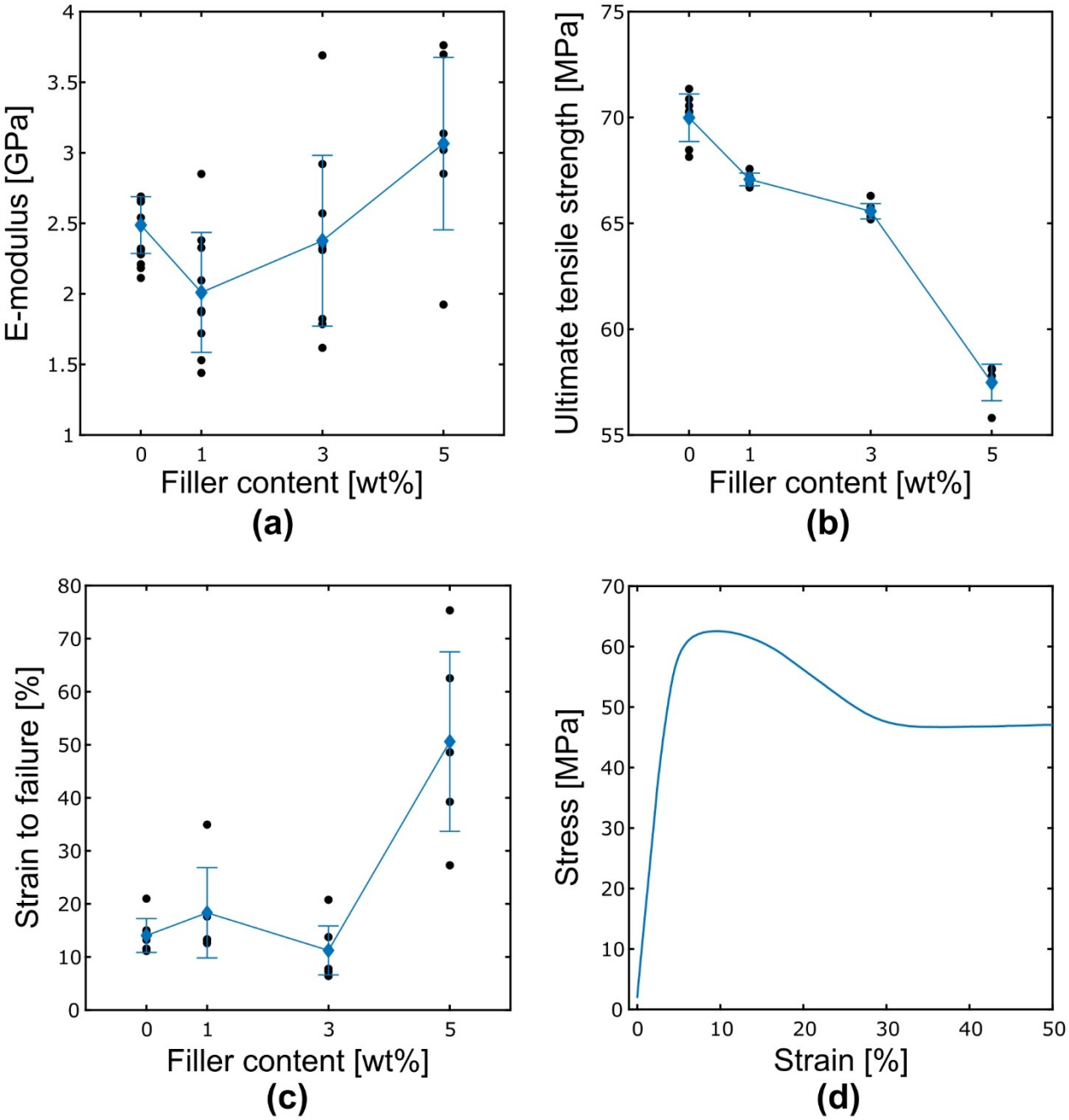

Figure 6. Experimentally determined tensile properties of pure epoxy and epoxy-SiO_2 nanocomposites with 1, 3 and 5 wt% SiO_2: (a) elastic modulus, (b) ultimate tensile strength, and (c) strain to failure. (d) shows a representative plot of the stress against the strain in the nanocomposites.

directly to how the nanocomposite system is built in the two models. In Model I, the spherical nanoparticle has a larger number of bonds than in Model II.

This affects the specific volume and, therefore, the density of the material at a given temperature. Although the thermal conductivity was not measured experimentally in this work, comparisons can be made with values reported in the literature. Mo et al.[28] reported a thermal conductivity of ~0.22 $W m^{-1} K^{-1}$ for pure epoxy. Kochetov et al.[29] reported thermal conductivities in epoxy-SiO_2 nanocomposites increasing from 0.168 to 0.199 $W m^{-1} K^{-1}$ with up to 15 wt% SiO_2. Zhang et al.[14] also performed MD simulations on epoxy-SiO_2 systems and demonstrated an increase in the thermal conductivity from 0.201 to 0.34 $W m^{-1} K^{-1}$ at 10 wt% SiO_2. The thermal conductivities calculated using Model I are larger but still comparable to the values reported in other works. Model II, however, presents significantly higher thermal conductivities that are closer to that of amorphous SiO_2 or SiO_2 films.[30,31] Both models exhibit the same trend observed in the literature, *i.e.*, the thermal

conductivity of the nanocomposites increases with increasing SiO_2 content.

Figure 6 shows the variations in the measured tensile elastic moduli, ultimate tensile strength, and the strain to failure in pure epoxy and SiO_2 nanocomposites (1, 3, and 5 wt%). The tensile elastic moduli of the nanocomposites exhibit the same behaviour observed using DMA, showing a decrease in the stiffness initially with 1 wt% SiO_2 (compared to pure epoxy), followed by a subsequent increase with higher SiO_2 content (3 and 5 wt%). The ultimate tensile strengths of the nanocomposites were lower than that of pure epoxy and decreased with increasing SiO_2 content.

The decrease in the tensile strength may be attributed to an increase in the brittleness of the polymer, as the inclusion of more fillers means potentially more defects in the composite. However, other works have shown that the tensile strength may be increased in the nanocomposites for low filler contents.[32] The strain to failure showed generally an increase with increasing filler content, most noticeably in the nanocomposites with the highest filler content (5 wt%), indicating increased ductility in the material prior to failure.

Using both models, the simulated tensile elastic moduli exhibit the same trend observed for the T_g – an initial decrease at lower filler content, followed by a subsequent increase with increasing filler content. However, the absolute values of the elastic moduli were better represented by each model for different conditions, as seen in Table 2. For low filler content (1 wt%), the modulus obtained from Model I was closer to the experimentally determined elastic moduli, whereas Model II was more accurate at a higher filler content (5 wt%).

Interestingly, the elastic modulus simulated for pure epoxy with cross-linking of ~90% was significantly higher than the experimentally determined modulus. The elastic modulus of epoxy with ~60% cross-linking was comparatively closer to the experimental value, albeit lower. The experimental T_g (from both DMA and DSC) of pure epoxy is likewise in between the T_g values predicted from the simulations for epoxy with 60% and 90% cross-linking. As seen previously in the tan δ (Figure 4b), the cross-linking in the epoxy is not homogeneous, and it is possible that certain regions of epoxy are not fully cross-linked. Changes in the cross-linking density of the nanocomposites are also expected depending on the state of dispersion of the SiO_2 nanoparticles, which is affected by the filler content. The DSC data does not exhibit a typical exothermic feature in the heat flow, which indicates that no cross-linking reactions are available for completion. Therefore, it can be assumed that the prepared samples are not completely cross-linked, but with a cross-linking degree closer to 70–80%, and this is the maximum limit due to the possibility of unreacted DGEBA and POPDA chains "frozen in" after a specific cross-linking limit is achieved.

The morphology of the fillers can also influence the mobility of the epoxy and curing agent molecules, thereby affecting the cross-linking degree and subsequently both T_g and the elastic moduli.

Conclusions

Models to represent epoxy-SiO_2 nanocomposites in MD simulations including all atomic interactions were developed. In Model I, the SiO_2 was represented as a nanoparticle with saturated bonds, and in a uniform distribution and in Model II, the SiO_2 was represented as simple molecules in a random dispersion with no bonds between the different molecules. Results from both models were quite consistent with the experimental results, exhibiting the same trends – both the glass transition temperature and the tensile elastic moduli initially decreased with small additions of SiO_2, but increased upon increasing the SiO_2 content further. Model II, however, returned poor estimates of the thermal conductivity of the nanocomposites compared to the Model I using SiO_2 as nanoparticles.

Radial distribution functions reveal that the SiO_2 as nanoparticles have an interfacial region extending to 3–5 nm from the particle surface. The interactions with the polymer chains are stronger, resulting in a higher coordination number of specific atoms in these chains around the SiO_2. The interfacial region is narrower for the molecular SiO_2, where a certain degree of clustering is observed among the molecules.

MD simulations can be quite accurate in describing the properties and structure of epoxy nanocomposites. However, specific models may be more suitable for predicting different properties under various conditions. It is likely that the most representative model for the SiO_2 nanoparticles in such a system would be a hybrid of the two used here – particles of SiO_2 with a defined size but spread randomly in the epoxy rather than in a fixed, uniform distribution. It should also be noted that in Model II some of the SiO_2 units can migrate into the polymer, and the potential is not parameterized for that environment. A more detailed or specialized force field would be required to mitigate this, which is a potential area for further development in this study. However, the force-field used in this work captures the SiO_2-polymer interactions sufficiently. Further developments of the model should also incorporate the possibility of bonded interactions at the particle-polymer interfaces, *e.g.*, with coupling agents. These models will complement the experimental measurements of the properties with a theoretical understanding of the structure-property relations in these materials.

Experimental and Computational Methods

The preparation of *in situ* epoxy-SiO_2 nanocomposites is described in a previous work.[25] Th e SiO_2 was synthesized *in situ* in epoxy using aminopropyltriethoxysilane as a coupling agent and tetraethylorthosilicate as the precursor for SiO_2 in an aqueous sol-gel process. The glass transition temperatures of the epoxy-SiO_2 nanocomposites were determined using both DSC and DMA. DSC was performed with four cycles of heating and cooling between 0 and 200 °C at 10 °C min^{-1}. DMA was performed using 3-point bending mode with a ramp rate of 3 °C min^{-1} from 30 °C to 120 °C in oscillation mode (1 Hz and 30 μm frequency). The tensile properties were measured according to the ASTM D638-14 standard at room temperature with a strain rate of 0.01 mm min^{-1}.

The structural models for the DGEBA and curing agent molecules were built using the OPLS-AA force-field with initial geometries obtained from LigParGen[23] and manually adjusted partial charges. A combination of the canonical (NVT) with the Nose-Hoover thermostat and isothermal-isobaric (NPT) ensembles was employed to relax and obtain the correct density of the system. A total of ~1300 molecules were used in the periodic simulation box. Cross-linking of the DGEBA and curing agent molecules was performed using a cut-off distance of 5 Å.

SiO_2 nanoparticles of various sizes in Model I were prepared by annealing a bulk structure with 64000 molecules using the NVT ensemble. Unsaturated bonds were terminated by hydroxyl groups. The nanoparticles were inserted into a central position in the periodic unit cell containing the epoxy monomers and curing agent. Individual SiO_2 (O–Si–O) molecules in Model II, corresponding to total filler contents of 1, 3, and 5 wt%, were inserted randomly into the simulation box together with monomers and a curing agent, followed by mixing in the NVT ensemble.

The glass transition behaviour of the simulated epoxy and epoxy-SiO_2 nanocomposites was observed from the change in density with temperature in a canonical ensemble. Tensile properties of the simulated systems were investigated by deformation of the unit cell with a fixed rate of 10^{-5} ps^{-1} over 0.1 ns along the x-axis. Thermal conductivities were modelled at 300 K and 1 atm using the OCTP plug-in for LAMMPS.[33] The RDFs were also calculated using the OCTP plug-in with calculations carried out in the micro-canonical (NVE) ensemble.

Further details on the equilibration of the systems, the cross-linking of the epoxy, the building of models for the epoxy and the SiO2, and the calculations of the thermal and mechanical properties are included in the Supplementary Information.

Acknowledgements

Financial support from The Research Council of Norway (RCN) through the project "Stipendiatstillinger til SINTEF Energi AS" (Project No. 259866) is acknowledged. AK and SKS acknowledge financial support from RCN through project No. 275754. Computational resources were provided thanks to Sigma2-The National Infrastructure for High Performance Computing and Data Storage in Norway (project NN9414K and NN9566K). MMA acknowledges support from Inger-Emma Nylund in taking the TEM images.

Conflict of Interest

The authors declare no conflict of interest.

Data Availability Statement

The data that support the findings of this study are available from the corresponding author upon reasonable request.

Keywords: epoxy · glass transition behaviour · molecular dynamics simulations · nanocomposites · thermomechanical properties

[1] J. K. Nelson, *Dielectric Polymer Nanocomposites*, Springer, New York, USA, **2010**.
[2] R. Kochetov, T. Andritsch, P. H. F. Morshuis, J. J. Smit, *IEEE Trans. Dielectr. Electr. Insul.* **2012**, *19*, 107–117.
[3] C. Calebrese, L. Hui, L. S. Schadler, J. K. Nelson, *IEEE Trans. Dielectr. Electr. Insul.* **2011**, *18*, 938–945.
[4] A. Bandyopadhyay, P. K. Valavala, T. C. Clancy, K. E. Wise, G. M. Odegard, *Polymer* **2011**, *52*, 2445–2452.
[5] G. M. Odegard, T. C. Clancy, T. S. Gates, *Polymer* **2005**, *46*, 553–562.
[6] A. Adnan, C. T. Sun, H. Mahfuz, *Compos. Sci. Technol.* **2007**, *67*, 348–356.
[7] B. S. Sindu, S. Sasmal, *Comput. Mater. Sci.* **2015**, *96*, 146–158.
[8] T. E. Gartner, A. Jayaraman, *Macromolecules* **2019**, *52*, 755–786.
[9] S. Sæther, M. Falck, Z. Zhang, A. Lervik, J. He, *Macromolecules* **2021**, *54*, 6563–6574.
[10] H. B. Fan, M. M. F. Yuen, *Polymer* **2007**, *48*, 2174–2178.
[11] J. Choi, S. Yu, S. Yang, M. Cho, *Polymer* **2011**, *52*, 5197–5203.
[12] V. Varshney, S. S. Patnaik, A. K. Roy, B. L. Farmer, *Macromolecules* **2008**, *41*, 6837–6842.
[13] P. H. Lin, R. Khare, *Macromolecules* **2009**, *42*, 4319–4327.
[14] X. Zhang, H. Wen, Y. Wu, *Polymers (Basel).* **2017**, *9*, 430.
[15] Q. Xie, K. Fu, S. Liang, B. Liu, L. Lu, X. Yang, Z. Huang, F. Lü, *Polymers (Basel)* **2018**, *10*, 801.
[16] J. Li, J. Chen, M. Zhu, H. Song, H. Zhang, *Appl. Sci.* **2019**, *9*, 2832.
[17] Z. Wang, Q. Lv, S. Chen, C. Li, S. Sun, S. Hu, *ACS Appl. Mater. Interfaces* **2016**, *8*, 7499–7508.
[18] O. Hölck, E. Dermitzaki, B. Wunderle, J. Bauer, B. Michel, *Microelectron. Reliab.* **2011**, *51*, 1027–1034.
[19] Y. L. Yaphary, Z. Yu, R. H. W. Lam, D. Hui, D. Lau, *Composites Part B* **2017**, *131*, 165–172.
[20] G. Zhao, J. Chen, Y. Lv, X. Zhang, L. Huang, *C. - Comput. Model. Eng. Sci.* **2021**, *128*, 339–357.
[21] K. Fu, F. Lü, Q. Xie, H. Ruan, X. Yang, S. Liang, *AIP Adv.* **2020**, *10*, 015339.
[22] D. Du, Y. Tang, L. Yang, C. Tang, *Polymers (Basel).* **2020**, *12*, 1662.
[23] L. S. Dodda, I. C. De Vaca, J. Tirado-Rives, W. L. Jorgensen, *Nucleic Acids Res.* **2017**, *45*, W331–W336.
[24] L. S. Dodda, J. Z. Vilseck, J. Tirado-Rives, W. L. Jorgensen, *J. Phys. Chem. B* **2017**, *121*, 3864–3870.
[25] M. M. Adnan, I.-E. Nylund, A. Jaworski, S. Hvidsten, M.-H. G. Ese, J. Glaum, M.-A. Einarsrud, *Polymers (Basel)* **2021**, *13*, 1469.
[26] M. M. Adnan, E. G. Tveten, R. Miranti, S. Hvidsten, M.-H. G. Ese, J. Glaum, M.-A. Einarsrud, *J. Sol-Gel Sci. Technol.* **2020**, *95*, DOI 10.1007/s10971-020-05220-3.
[27] P. Judeinstein, C. Sanchez, *J. Mater. Chem.* **1996**, *6*, 511–525.
[28] H. Mo, X. Huang, F. Liu, K. Yang, S. Li, P. Jiang, *IEEE Trans. Dielectr. Electr. Insul.* **2015**, *22*, 906–915.
[29] R. Kochetov, A. V. Korobko, T. Andritsch, P. H. F. Morshuis, S. J. Picken, J. J. Smit, *J. Phys. D* **2011**, *44*, 395401.
[30] W. Zhu, G. Zheng, S. Cao, H. He, *Sci. Rep.* **2018**, *8*, 10537.
[31] T. Yamane, N. Nagai, S. I. Katayama, M. Todoki, *J. Appl. Phys.* **2002**, *91*, 9772–9776.
[32] M. M. Adnan, E. G. Tveten, J. Glaum, M.-H. G. Ese, S. Hvidsten, W. Glomm, M.-A. Einarsrud, *Adv. Electron. Mater.* **2019**, *5*, 1800505.
[33] S. H. Jamali, L. Wolff, T. M. Becker, M. De Groen, M. Ramdin, R. Hartkamp, A. Bardow, T. J. H. Vlugt, O. A. Moultos, *J. Chem. Inf. Model.* **2019**, *59*, 1290–1294.

Manuscript received: June 24, 2022
Revised manuscript received: March 8, 2023
Accepted manuscript online: March 8, 2023
Version of record online: March 28, 2023